Hindawi
Journal of Control Science and Engineering
Volume 2019, Article ID 1480732, 13 pages
https://doi.org/10.1155/2019/1480732

Research Article

Comparative Analysis of Neural-Network and Fuzzy Auto-Tuning Sliding Mode Controls for Overhead Cranes under Payload and Cable Variations

Muhammad A. Shehu, Ai-jun Li, Bing Huang, Yu Wang, and Bojian Liu

Control and Information Engineering, School of Automation, Northwestern Polytechnical University, Xi'an, Shaanxi 710072, China

Correspondence should be addressed to Muhammad A. Shehu; shehu.muhammad@mail.nwpu.edu.cn

Received 25 September 2018; Revised 7 November 2018; Accepted 19 December 2018; Published 3 January 2019

Guest Editor: Le Anh Tuan

The overhead crane is required to operate fast and precisely with minimal sway. However, high-speed operations cause undesirable load sways, hazardous to operating personnel, the payload being handled, and the crane itself. Thus, a high-quality control is required. In this work, the nonlinear model of the overhead crane was established and the sliding mode control (SMC) was proposed that ensured the existence of sliding motion in the presence of payload and hoisting height variations, and viscous frictions. To maximize the benefits derived from the proposed control method, novel sliding slope-update based on intelligent neural-network and fuzzy algorithms were developed to tune the controller, guaranteeing precise tracking of the actuated variables as well as regulation of the unactuated variables. The proposed methods adjust predetermined value of the sliding manifold's slope in response to variations in hoisting heights. Control applications were conducted, and results based on graphical, integral absolute error (IAE), and integral time absolute error (ITAE) proved the effectiveness of the proposed algorithms. It was observed that the response of the controller with back-propagation-trained neural-network was more effective relative to that of the fuzzy algorithm.

1. Introduction

The overhead crane, the tower crane, and the boom crane are the most common types of cranes in use today. Among other crane systems, the modern overhead crane is increasingly becoming more popular due to its cost-effectiveness and ease of operation. The crane is used in the transport industry for loading and unloading freight, in the construction industry for material and equipment handling, and in shipping yards for loading and unloading cargo. Other important areas of crane application include the mining sites, power plants, warehouses, the manufacturing industry [1], and other applications where human power is not a solution.

Like other crane systems, the overhead crane is required to operate precisely with high-speed, and with the absence or minimal sway for improved productivity and safety reasons. However, high-speed operations without a high-quality control strategy cause undesirable payload swings and positioning inaccuracies. The operator is able to decrease such hazardous swings by moving the cart in small increments; however, manual operation may result in increased operation time and operator workload. As a result, there is the need for automation and optimization of crane operation. The control problem is challenging due to the underactuated nature of the system. Other factors that significantly affect control quality include modeling errors, deliberately neglected nonlinearities, parametric variations, and disturbances.

Among research interests, the requirement for a high-quality controller to precisely drive the crane with minimal payload swings has attracted attentions and many constructive results have been published. Broadly, the existing control strategies in literature can be categorized into three: open-loop (OL), closed-loop (CL), and hybrid control (HC) schemes. For the OL schemes, the input command shaping (ICS) [2–8], the filter control [9], the command smoothing techniques (CS) [10], and the trajectory planning (TP) techniques [11–13] had been proposed. ICS achieves sway minimization by exciting two or more transient oscillations at different instances that result in effective cancellation of the payload oscillations. For the filter technique, the infinite

impulse response (IIR) filter was proposed by [9], where the effectiveness of 3rd-, 6th-, and 9th-order Butterworth low-pass and band-stop IIR filters was studied. Filtering is developed on the basis of extracting input energy around system's natural frequencies, preprocessing the signal so that no energy at system's natural frequency is fed into the system. The CS method was proposed in [10] for limiting vibration in crane systems by a way of smoothing the original reference command. The input command is smoothed to drive the crane without inducing payload oscillations. It has been noticed that the CS technique proposed by [10] was more robust at relatively higher frequencies compared to the ICS methods. On the other hand, the ICS methods were more robust at relatively lower frequencies compared to the CS technique. For the proposed TP techniques, energy efficiency of transportation has seldom been considered in planning trajectories. Wu and Xia [13] exploited this consideration and developed an optimal solution of trajectory planning in terms of energy efficiency for overhead cranes. It is worth pointing out that OL techniques focus only on the suppression of the acceleration-induced payload sways. Nonetheless, the merits of OL control techniques include ease of implementation and no extra feedback sensors are required. Also, for the case of robust ICS, there may be additional time delays due to delaying of the command signal. Moreover, OL techniques are sensitive to external disturbances [14].

Closed-loop techniques on the other hand achieve position tracking and sway suppression using feedback information to generate the right control signal(s). Several CL solutions have been developed for control of cranes. The proportional-integral control (PID) was proposed by [15–17] and positive results were obtained. For the PID techniques, the authors used a PID controller for position control and a PD controller for sway suppression. Control techniques using optimal linear quadratic regulator (LQR) were proposed by [8] and constructive results were obtained using linearized crane model. Sun et al. [18] developed an adaptive anti-swing control strategy for uncertain double-pendulum cranes. In another work published by [19], the fuzzy logic control was proposed. Control using fuzzy logic has a strong adaptability and does not require obtaining an accurate crane model. The pole placement control was proposed by the authors in [20] where several control applications were conducted to investigate the performances of three different sets of system poles based on time response criteria. The model predictive control (MPC) was proposed by Wu et al. [21]. The SMC control (which is the focus of this work) had been studied in [1, 22–32]. SMC is a special type of variable structure control characterized by a discontinuous control structure that switches as the system crosses certain manifold in the state-space to drive the system trajectory to reach and subsequently remain on the sliding manifold within the state space [33]. In [21] the SMC controller was used to control two degrees of freedom (DOFs): cart poison and payload sway, where two sliding manifolds were designed for each DOF. The authors proposed the fuzzy logic algorithm to dynamically adjust a coupling parameter between the two manifolds. A method of combining SMC was proposed by [1]; an intermediate variable was introduced by a way of dividing system states into two groups and then defining a manifold on the basis of the intermediate variable. In this way, the number of states variables to consider for design gets reduced. Consequently, the manifold complexity also gets reduced. Simulation results proved the feasibility of the intermediate variable approach. The integral SMC for discrete-time systems was proposed by [23]. The SMC with moving sliding manifold was proposed by [24] where adaptive neurofuzzy inference system was used to generate the value of the manifold slope. The authors in [25–28, 30] proposed adaptive SMC for overhead cranes with uncertainties. The second-order SMC was proposed by [26]. The major advantage of second-order SMC is eliminating the so-called chattering effect by having a continuous control effort. Other techniques that hybridize different control schemes had also been proposed in the literature [34–36]. The interested reader may find the feedback linearization with the SMC in [34], the PID hybridized with fuzzy SMC by Hai et al. [35], and the adaptive NN SMC by Tuan et al. [36], to name a few.

In this study, the effectiveness of neural-network (NN) and fuzzy auto-tuning SMC techniques designed to update predetermined value of manifold's slope parameter are compared. Based on this "update-approach," there would be no singularity in the controller when the tuning system fails as could be the case using the "generate-approach" of the author in [24]. To the best of the authors' knowledge, this is the first publication where the NN-based and fuzzy-based auto-tuning SMC algorithms are compared. Studies have shown that optimizing the SMC yields improved performance [24] regarding convergence and fast vanishing of residual sway.

The rest of the paper organization is as follows. Mathematical modelling of the system is presented in Section 2. Section 3 is devoted to the design of the proposed control strategy, and the intelligent NN-based and fuzzy-based SMC tuning algorithms. Section 4 is devoted to the applications of the proposed control methods, as well as the performance evaluations of the proposed methods based on graphical, IAE, and ITAE criteria. Section 5 concludes the paper.

2. Mathematical Modelling

As shown in Figure 1, the system under study is a two-dimensional overhead crane. The parameters and variables that describe the system are defined in Table 1. Derivation of the mathematical model for the system is based on the Euler-Lagrange method. For modelling simplicity, the following assumptions are considered.

Assumption 1. Mass of hoisting cable is insignificant, all rotating joints are well lubricated, hoisting is only needed for obstacle avoidance, and all-states are available for control design.

From Figure 1, the x- and y-coordinates of the payload (x_p, y_p) and their corresponding time-derivatives can be written as

$$x_p = x + L\sin\varphi,$$

$$\dot{x}_p = V_x = \dot{x} + L\dot{\varphi}\cos\varphi,$$

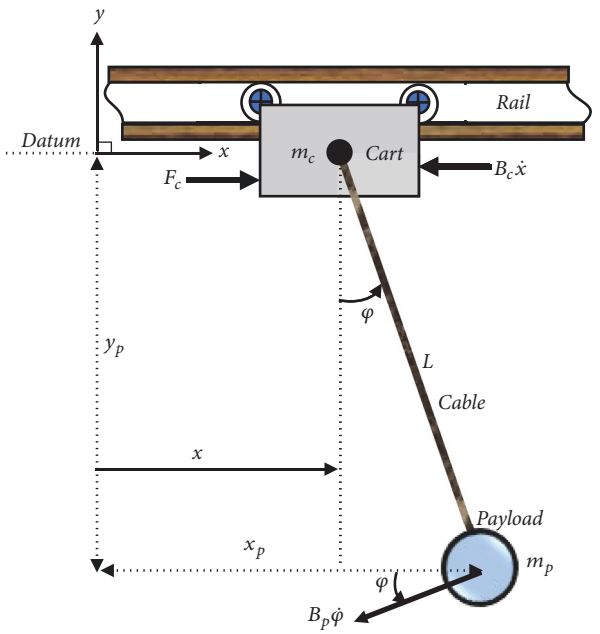

Figure 1: System schematic diagram. The motor is assumed stopped and the payload was at an angle.

Table 1: Dynamics model parameters.

Notation	Description	Unit
m_c	Mass of driving cart	kg
m_p	Mass of payload	kg
L	Length of hoisting cable	m
B_c	Cart's viscous damping coefficient	N-s/m
B_p	Payload's viscous damping coefficient	N-m-s/rad
φ	Payload sway angle	rad
$\dot{\varphi}$	Payload sway angular velocity	rad/s
x	Driving cart's position	m
$\dot{x}$	Driving cart's linear velocity	m/s
F_c	Cart control force	N
r_p	Radius of cart's pulley	m
R	Motor electrical resistance	Ω
T_m	DC motor torque	Nm
K_m	DC motor torque constant	Nm/A
V_{DC}	Dc motor input voltage	V
K_E	DC motor electric constant	V/rad/s

$$\begin{aligned} y_p &= -L\cos\varphi, \\ \dot{y}_p &= V_y = L\dot{\varphi}\sin\varphi. \end{aligned} \tag{1}$$

System equations-of-motion (EOM) are obtained using Euler-Lagrange equation given by

$$\begin{aligned} \frac{d}{dt}\left(\frac{\partial L_a}{\partial \dot{q}_i}\right) - \left(\frac{\partial L_a}{\partial q_i}\right) &= Q_i - Q_i^{Lost}, \quad i = 1, 2\ldots, n \\ L_a &= T - P, \end{aligned} \tag{2}$$

where $T = KE_{crane}$ and $P = PE_{crane}$, Q_i is a vector of nonconservative generalized forces acting along the direction of the generalized coordinates q_i, and n is the number of independent generalized coordinates. For this study, the independent generalized coordinates in (2) are defined as $q \triangleq [q_1 \;\; q_2]^T = [x \;\; \varphi]^T$, while the nonconservative generalized forces are defined as $Q \triangleq [Q_1 \;\; Q_2]^T = [F_c \;\; 0]^T$ and the lost terms as $Q^{Lost} = [B_c\dot{x} \;\; B_pL\dot{\varphi}]^T$.

The EOM for the system can be summarized in matrix form as

$$\begin{aligned} &\begin{bmatrix} (m_c + m_p) & m_pL\cos\varphi \\ \cos\varphi & L \end{bmatrix} \begin{bmatrix} \ddot{x} \\ \ddot{\varphi} \end{bmatrix} \\ &\quad + \begin{bmatrix} 0 & -m_pL\dot{\varphi}\sin\varphi \\ 0 & 0 \end{bmatrix} \begin{bmatrix} \dot{x} \\ \dot{\varphi} \end{bmatrix} + \begin{bmatrix} 0 \\ g\sin\varphi \end{bmatrix} \\ &= \begin{bmatrix} F_c - B_c\dot{x} \\ -B_p\dot{\varphi}, \end{bmatrix}. \end{aligned} \tag{3}$$

The term $B_c\dot{x}$ opposes the cart force, F_c, and refers to the viscous damping of the driving cart due to friction between the cart and air. Similarly, the viscous damping term $B_p\dot{\varphi}$ refers to the viscous damping force of the swinging payload, given by the friction between payload and air.

It is evident that the EOM for the system presented as (3) are coupled in the actuated acceleration variable $\ddot{x}$ and the unactuated acceleration variable $\ddot{\varphi}$. The EOM can be decoupled into actuated and unactuated subsystems. Isolating $\ddot{\varphi}$ and $\ddot{x}$ from (3), we have

$$\ddot{x} = \frac{F_c - B_c\dot{x} + m_pg\sin\varphi\cos\varphi + m_pL\dot{\varphi}^2\sin\varphi + B_p\dot{\varphi}\cos\varphi}{(m_c + m_p) - m_p\cos^2\varphi}, \tag{4}$$

$$\ddot{\varphi} = \frac{-(m_c + m_p)(m_pg\sin\varphi + B_p\dot{\varphi}) - F_cm_p\cos\varphi + m_p\cos\varphi(B_c\dot{x} - m_pL\dot{\varphi}^2\sin\varphi)}{m_pL(m_c + m_p - m_p\cos^2\varphi)}. \tag{5}$$

By noting that the variables notations $x_1 = x$, $x_2 = \dot{x}$, $x_3 = \varphi$, and $x_4 = \dot{\varphi}$ apply, the EOM for the crane system (see (4) and (5)) can be presented as

$$\begin{aligned} \dot{x}_1 &= x_2, \\ \dot{x}_2 &= f_1(x) + g_1(x)F_c, \end{aligned}$$

$$\dot{x}_3 = x_4,$$
$$\dot{x}_4 = f_2(x) + g_2(x) F_c, \tag{6}$$

with

$$f_1(x) = \frac{\left(B_c\dot{x} + m_p g \sin\varphi\cos\varphi + m_p L\dot{\varphi}^2 \sin\varphi + B_p\dot{\varphi}\cos\varphi\right)}{\left(m_c + m_p - m_p\cos^2\varphi\right)},$$
$$g_1(x) = \frac{1}{\left(m_c + m_p - m_p\cos^2\varphi\right)},$$
$$f_2(x) = \frac{\Gamma}{m_p L\left(m_c + m_p - m_p\cos^2\varphi\right)}, \tag{7}$$
$$g_2(x) = \frac{-m_p\cos\varphi}{m_p L\left(m_c + m_p - m_p\cos^2\varphi\right)},$$
$$\Gamma = -\left(m_c + m_p\right)\left(m_p g\sin\varphi + B_p\dot{\varphi}\right) + m_p\cos\varphi\left(B_c\dot{x} - m_p L\dot{\varphi}^2\sin\varphi\right).$$

In (6), the linear force, F_C, that drives the cart originates from the trolley DC motor torque. Taking the effect of DC motor dynamics into account, the following equations relating the linear force F_C to motor torque T_m, and motor input voltage V_{DC}, are defined

$$T_m = r_p F_C = \frac{K_m}{R_m}V_{DC} - \frac{K_m K_E}{R_m}\omega_m,$$
$$\omega_m = \frac{x_2}{r_p} \tag{8}$$

where r_p, K_m, V_{DC}, K_E, and R_m have been defined earlier in Table 1, while ω_m refers to the angular velocity of the motor. From (8), one easily isolates F_C as

$$F_C = \frac{K_m}{R_m r_p}V_{DC} - \frac{K_m K_E}{R_m {r_p}^2}x_2 \tag{9}$$

In Section 3, we present the design of the proposed control strategy. The following assumption is considered for control design.

Assumption 2. The nonlinear functions $g_1(x)$ and $g_2(x)$ are assumed to be invertible $\forall x$.

3. Control System Design and Stability Analysis

The problem is to transport the payload along the desired trajectory from an initial position to the final position in short time with no or attenuated sway. These conflicting requirements coupled with the underactuated nature of the crane make the control more challenging. The SMC is proposed for the crane control problem. To optimize the performance of the proposed controller, intelligent tuning systems based on the NN and the fuzzy logic will be designed.

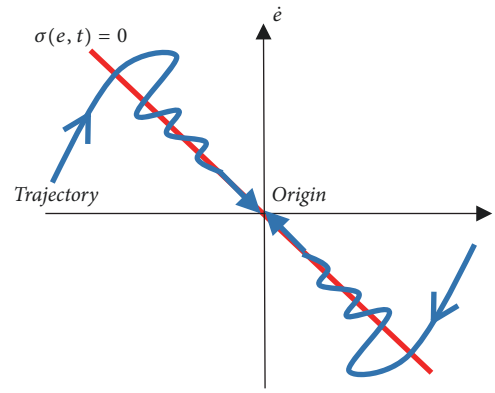

Figure 2: Attractive property of the sliding manifold.

3.1. Sliding Mode Control Design and Stability Analysis. SMC is a special type of variable structure system where control law is designed to drive system trajectory to reach and remain on a designed manifold within the state-space called sliding manifold [33]. As shown in Figure 2, the error trajectory after the initial *reaching phase* "slides" on the manifold $\sigma(e,t) = 0$. Insensitivity to parametric and matched uncertainties and disturbance make the SMC particularly attractive in robust control.

For the second-order actuated subsystem, design the sliding manifold as

$$\sigma(e,t) = C^T e, \tag{10}$$

where $e \triangleq \left[e \;\; \dot{e}\right]^T = \left[e_1 \;\; e_2\right]^T$ is error vector and C^T is sliding manifold parameters vector that characterizes the manifold. The position error, e_1, has been defined as $e_1 = x_1 - x_1^d$, while the velocity error, e_2, has been defined as $e_2 = x_2 - x_2^d$. The variables x_1 and x_2 represent the actual system trajectories with desired trajectories as x_1^d and x_2^d, respectively. Without loss of generality, define $C^T = \left[C_1 \;\; 1\right]^T$; hence, (10) and its time-derivative are, respectively, given by

$$\sigma(e,t) = C_1\left(x_1 - x_1^d\right) + \left(x_2 - x_2^d\right). \tag{11}$$

$$\dot{\sigma}(e,t) = C_1\left(\dot{x}_1 - \dot{x}_2^d\right) + \left(\dot{x}_2 - \dot{x}_2^d\right). \tag{12}$$

All velocities are zero at steady state; hence, set $\dot{x}_1^d = x_2^d = \dot{x}_2^d = 0$. Eventually, submitting the crane system given by (6) into (12) we have

$$\dot{\sigma}(e,t) = C_1\dot{x}_1 + \dot{x}_2 = C_1 x_2 + f_1(x) + g_1(x) F_c. \tag{13}$$

Parameter C_1 is designed for the polynomial $p+C_1 = 0$ to be Hurwitz, where p is a Laplace operator. Thus, it is required that $C_1 > 0$. We adopt the equivalent control given by

(14) where u_{eq} and u_{sw} are known as the equivalent and the switching control, respectively.

$$F_c = u_{eq} + u_{sw}. \tag{14}$$

During the *sliding phase*, only u_{eq} control is applied to maintain the trajectories sliding along $\sigma(e,t) = 0$. However, during *reaching phase*, both u_{eq} and u_{sw} make the total control law, F_c. During sliding, $\dot{\sigma}(e,t) = 0$ exists. Hence, considering (13), u_{eq} is designed as

$$u_{eq} = \frac{-\left(C_1 x_2 + f_1(x)\right)}{g_1(x)}. \tag{15}$$

We will design u_{sw} from stability analysis. Define the candidate Lyapunov function as

$$V(\sigma,t) = \frac{1}{2}\sigma(e,t)^2. \tag{16}$$

One may have noticed that the selection of the Lyapunov function satisfies the stability requirements that $V(\sigma,t) = 0$ for $\sigma = 0$ and $V(\sigma,t) > 0$ for $\sigma \neq 0$ $\forall t$. By differentiating (16) with respect to time along (15) one arrives at

$$\begin{aligned} \dot{V}(\sigma,t) &= \sigma(e,t)\,\dot{\sigma}(e,t) \\ &= \sigma(e,t)\left(C_1 x_2 + f_1(x) + g_1(x)F_c\right). \end{aligned} \tag{17}$$

By submitting (14) and (15) into (17) and simplifying, (17) reduces to

$$\dot{V}(\sigma,t) = \sigma(e,t)\,g_1(x)\,u_{sw}. \tag{18}$$

In (18), for the system to be asymptotically stable, it is required that $\dot{V}(\sigma,t) < 0$ holds. Note that the factor $g_1 = 1/(m_c + m_p - m_p\cos^2\varphi)$ in (18) is strictly positive. Hence, the values that the switching law u_{sw} is set to achieve $\dot{V}(\sigma,t) \leq 0$ are given as

$$u_{sw}\begin{cases} > 0 & if\ \sigma(e,t) < 0, \\ = 0 & if\ \sigma(e,t) = 0, \\ < 0 & if\ \sigma(e,t) > 0, \end{cases} \tag{19}$$

and by LaSalle's invariance principle [37] we have $\dot{V}(\sigma,t) < 0$ and the crane is asymptotically stable about the origin. To meet the requirements of (19), design u_{sw} as

$$u_{sw} = -\xi\,\mathrm{sign}(\sigma(e,t)), \tag{20}$$

where ξ is a positive constant and the signum function sign$(\cdot)$ is defined as

$$\mathrm{sign}(\sigma(e,t)) := \begin{cases} -1 & if\ \sigma(e,t) < 0, \\ 0 & if\ \sigma(e,t) = 0, \\ 1 & if\ \sigma(e,t) > 0. \end{cases} \tag{21}$$

Remark 3. To reduce the fast switching of the control law, we replace sign$(\cdot)$ by the smoothing function [38] given by (22), where $\delta > 0$. Here $\delta = 0.05$ is selected. The smoothing function eliminates the fast switching of the control law while preserving robustness property around some neighbourhood of the sliding manifold.

$$\mathrm{sign}(\sigma(e,t)) \approx \frac{\sigma(e,t)}{|\sigma(e,t)| + \delta} \tag{22}$$

In this study, the controller parameters are designed as $\xi = 70$ and $C_1 = 5.48$. The closed-loop system will maintain robust stability against matched and parametric uncertainties. However, as stated earlier, high-speed operation coupled with variations in hoisting heights may affect the *reaching time* to $\sigma(e,t) = 0$ for sway. Linearizing (5) about $\varphi = 0^0$, one obtains

$$\ddot{\varphi} + \frac{B_p}{Lm_p}\dot{\varphi} + \frac{g}{L}\varphi = -\frac{1}{L}\ddot{x}. \tag{23}$$

Equation (23) represents a second-order system. When expressed in transfer function form, it can be easily proved that the undamped-natural frequency, ω_n, of the crane is given by

$$\omega_n = \sqrt{\frac{g}{L}}. \tag{24}$$

In (24), it is evident that ω_n is L-dependent. Changes in L are likely to affect the swaying duration. Studies show that optimizing the SMC yields improved performance [24] regarding convergence and fast vanishing of residual sway. In this study, we compare the intelligent NN and fuzzy logic algorithms for tuning the slope parameter C_1 of the controller. The approach to the SMC optimization problem in this study is to design intelligent systems to update the previously designed slope parameter C_1 (here redefined as C_1^0) according to

$$C_1 = C_1^0 + \Delta C_1 \tag{25}$$

It is to be noted that our approach is different from that proposed by [24] where neurofuzzy system was proposed to generate the slope parameter C_1. In this work, the intelligent system updates predetermined value of C_1 by an amount ΔC_1 (determined by the intelligent system) rather than completely generating it. Hence, there would be no singularity in the slope parameter C_1 when the intelligent system fails as may be the case using the "slope-generate" approach of [24]. Using the "slope-update" approach, the system will remain operational (although with reduced effectiveness) even when intelligent tuning system fails.

3.2. Intelligent Tuning Algorithms Designs. Optimal training dataset was obtained through tuning exercises for different sets of hoisting heights in the range 0.25 meters to 1.5 meters. The knowledge from the tuning exercise was used to carry out supervised training of the NN and to design the fuzzy algorithm. The control architecture is as shown in Figure 3. The switch, *Sw*, is used to select the algorithm of choice. The outputs of the intelligent algorithms adjust controller slope for all operating conditions.

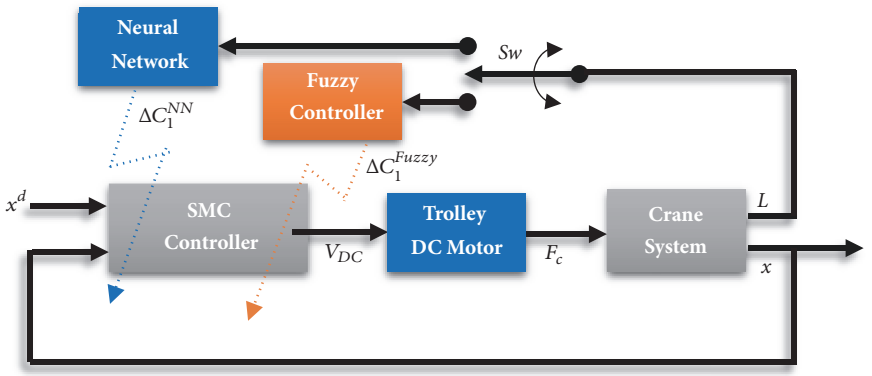

Figure 3: Closed-loop system block diagram with proposed intelligent SMC tuning algorithms.

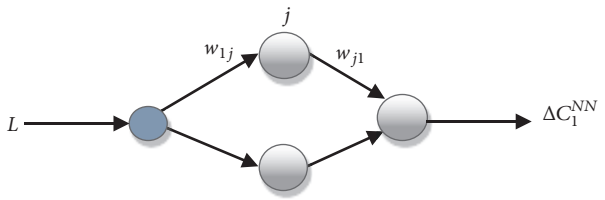

Figure 4: Neural-network architecture.

3.2.1. Neural-Network Design. As shown in Figure 4, the NN is a feed-forward, two-layered network with a 1-2-1 structure. The input node takes in the hoisting height data. The weighting factor linking the input node to the jth hidden-layer is denoted by w_{1j}, while the weighting factor linking the jth hidden-layer to the output-layer is denoted by w_{j1}. The network output is change in slope, ΔC_1^{NN}.

Define the instantaneous error between the desired change in slope (ΔC_1^d) and the NN-based change in slope (ΔC_1^{NN}) as

$$e(k) = \Delta C_1^d(k) - \Delta C_1^{NN}(k) \tag{26}$$

Since the network's output (ΔC_1^{NN}) can be positive, negative, or zero, the hidden- and the output-layers use the *tangent hyperbolic* activation function defined as

$$f_{h,o}(net) = \frac{e^{net} - e^{-net}}{e^{net} + e^{-net}}. \tag{27}$$

The input gets multiplied by the weights w_{1j} linking the input node to the hidden-layer. The summation of the product operations is the input to the hidden-layer neurons given by

$$I_j = \sum w_{1j} L. \tag{28}$$

The output from the jth neuron in the hidden-layer can be expressed as

$$O_j = f_{h,o}(I_j), \quad (j = 1, 2). \tag{29}$$

The output of the jth hidden-layer neuron gets multiplied by the weight w_{j1}. Contributions from all nodes are sent to the output-layer neuron according to

$$I_o = \sum w_{j1} O_j, \quad (j = 1, 2). \tag{30}$$

The output from the neuron in the output-layer is given by

$$\Delta C_1^{NN} = f_{h,o}(I_o). \tag{31}$$

Adaptation of the network weights is by the steepest descent back-propagation algorithm [39]. Define the cost function (to be minimized) as mean squared of the training error given by

$$J(k) = e(k) = \frac{1}{2}\left\{\Delta C_1^d(k) - \Delta C_1^{NN}(k)\right\}^2. \tag{32}$$

Generally, adjustment of each weight linking hidden-layer to output-layer can be expressed as

$$\Delta w_{j1}(k) = -\eta \frac{\partial J(k)}{\partial w_{j1}} + \gamma \Delta w_{j1}(k-1), \tag{33}$$

where η and γ are positive constants known as the learning and the momentum factor, respectively. γ is to avoid the solution from getting trapped in the so-called *local minima* [40]. In (33), the partial derivative $\partial J(k)/\partial w_{jk}$ can be expressed based on the chain rule as

$$\frac{\partial J(k)}{\partial w_{j1}} = \frac{\partial J(k)}{\partial \Delta C_1^{NN}(k)} \cdot \frac{\partial \Delta C_1^{NN}(k)}{\partial I_o(k)} \cdot \frac{\partial I_o(k)}{\partial w_{j1}(k)}. \tag{34}$$

Next, we define the partial derivatives in (34). From (30), it happens that

$$\frac{\partial I_o(k)}{\partial w_{j1}(k)} = O_j(k). \tag{35}$$

Also, considering (31), the following can be obtained:

$$\frac{\partial \Delta C_1^{NN}(k)}{\partial I_o(k)} = f_{h,o}'(net) = f_{h,o}(net)\left(1 - f_{h,o}(net)\right). \tag{36}$$

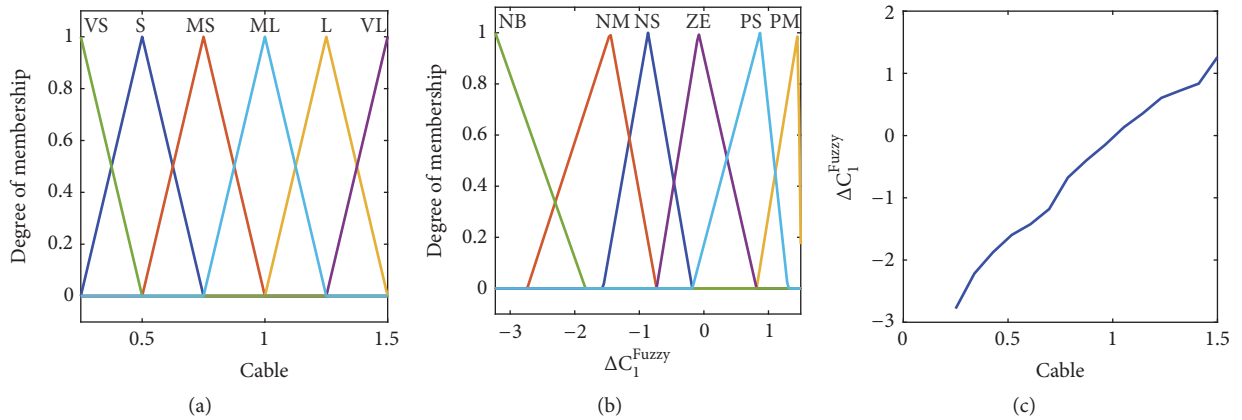

Figure 5: Fuzzy: (a) input MFs; (b) output MFs; (c) input-output characteristics.

Similarly, considering (32), it can also be verified that

$$\frac{\partial J(k)}{\partial \Delta C_1^{NN}(k)} = -e(k). \tag{37}$$

Putting all defined derivatives together, (34) is given by

$$\frac{\partial J(k)}{\partial w_{j1}} = -e(k) \cdot {f_{h,o}}'(net) \cdot O_j(k). \tag{38}$$

Finally, the update algorithm for the next output-layer weights, $w_{j1}(k+1)$, is given by

$$w_{j1}(k+1) = w_{j1}(k) + \Delta w_{j1}(k) + \gamma \Delta w_{j1}(k-1) \tag{39}$$

By applying similar sets of calculations (see (33)-(39)) for the output-layer, the hidden-layer weights are updated according to the update rule given by

$$w_{1j}(k+1) = w_{1j}(k) + \Delta w_{1j}(k), \tag{40}$$

where in this case the change in the jth hidden-layer weight has been defined as

$$\Delta w_{1j}(k) = -\eta . f'_{h,o}(net)\, e(k) . f'_{h,o}(net) . \sum w_{j1} . L + \gamma . \Delta w_{1j}(k-1). \tag{41}$$

3.2.2. Fuzzy Algorithm Design. The input is hoisting height, L, while the output is ΔC_1^{Fuzzy}. Triangular membership functions (MFs) are selected for the input and output variables as shown in Figures 5(a) and 5(b), respectively. The input takes the linguistic values: **VS**: Very Short (L is about 0.25 meters), **S**: Short (L is about 0.5 meters), **MS**: Medium Short (L is about 0.75 meters), **ML**: Medium Long (L is about 1 meter), **L**: Long (L is about 1.25 meters), and **VL**: Very Long (L is about 1.5 meters). The output is assumed to take the following linguistic values: **NB** (Negative Big), **NM** (Negative Medium), **NS** (Negative Small), **ZE** (zero), **PS** (Positive Small), and **PM** (Positive Medium).

The first step is to take the crisp hoisting height input and determine its degree of belonging in each of the fuzzy sets via MFs. Since we have single input and single output system, the rule antecedent and consequent parts are simple. The ith linguistic rule set can be expressed as

$$R^i\text{: IF } L \text{ is } M^i \text{ THEN } \Delta C_1^{Fuzzy} \text{ is } N^i, \quad i = 1, 2, \ldots, n \tag{42}$$

where R^i is the i^{th} rule of the n rules and M^i and N^i are the corresponding MFs for L and ΔC_1^{Fuzzy}. The one-dimensional rule is given by Table 2. Defuzzification for obtaining the crisp output is based on the following simplified inference method where $\mu_{M^i}(L)$ is the firing strength of the i^{th} rule.

$$\Delta C_1^{Fuzzy} = \frac{\sum_i^n \mu_{M^i}(L) \times N^i}{\sum_i^n \mu_{M^i}(L)}, \tag{43}$$

In Figure 5(c), the near-linear relationship between the crisp cable length and the crisp output ΔC_1^{Fuzzy} is shown. The crisp output ΔC_1^{Fuzzy} is used to update the SMC slope parameter according to (25).

Table 2: One-dimensional rule table for fuzzy tuning algorithm.

Input:	VS	S	MS	ML	L	VL
Output:	NB	NM	NS	ZE	PS	PM

4. Applications of the Designed Control Algorithms

The parameters of the model are accepted as in Table 3. Payload changes according to the mass of the load to be transported. The hoisting height also changes during loading and unloading and when avoiding obstacles. The natural frequency of the system changes as cable length changes; thus the sway characteristic of the system changes. Changes in hoisting height are likely to cause deterioration in sway suppression. For these reasons, control applications were repeated by varying payload and hoisting height to demonstrate the effectiveness of the proposed control strategy with the designed intelligent tuning algorithms.

Table 3: Numerical values for the simulation model parameters.

Parameter:	m_c[kg]	B_c[Ns/m]	B_p[Nms/rad]	r_p[m]	R[Ω]	K_m[Nm/A]	K_E[V/rad/s
Value:	25	0.25	0.1	0.07	3.35	0.24	0.24

Table 4: Fuzzy-SMC and neural network-SMC comparisons based on IAE and ITAE.

	System Configuration			IAE		ITAE	
Case ID	Cart ref. [m]	Cable [m]	Payload [kg]	FZ-SMC	NN-SMC	FZ-SMC	NN-SMC
1	1	1.25	5	0.1745	0.1744	0.2249	0.2245
2	2	1⟶1.5⟶0.5	10	0.4118	0.4115	1.5060	1.5010
3	1⟶2⟶3	1	20	0.7418	0.7416	9.7370	9.7330
4	1⟶2⟶3	1⟶1.5⟶0.5	20	0.7769	0.7754	10.8100	10.7700
5	1	1.7	15	0.5489	0.1653	4.6300	0.3695

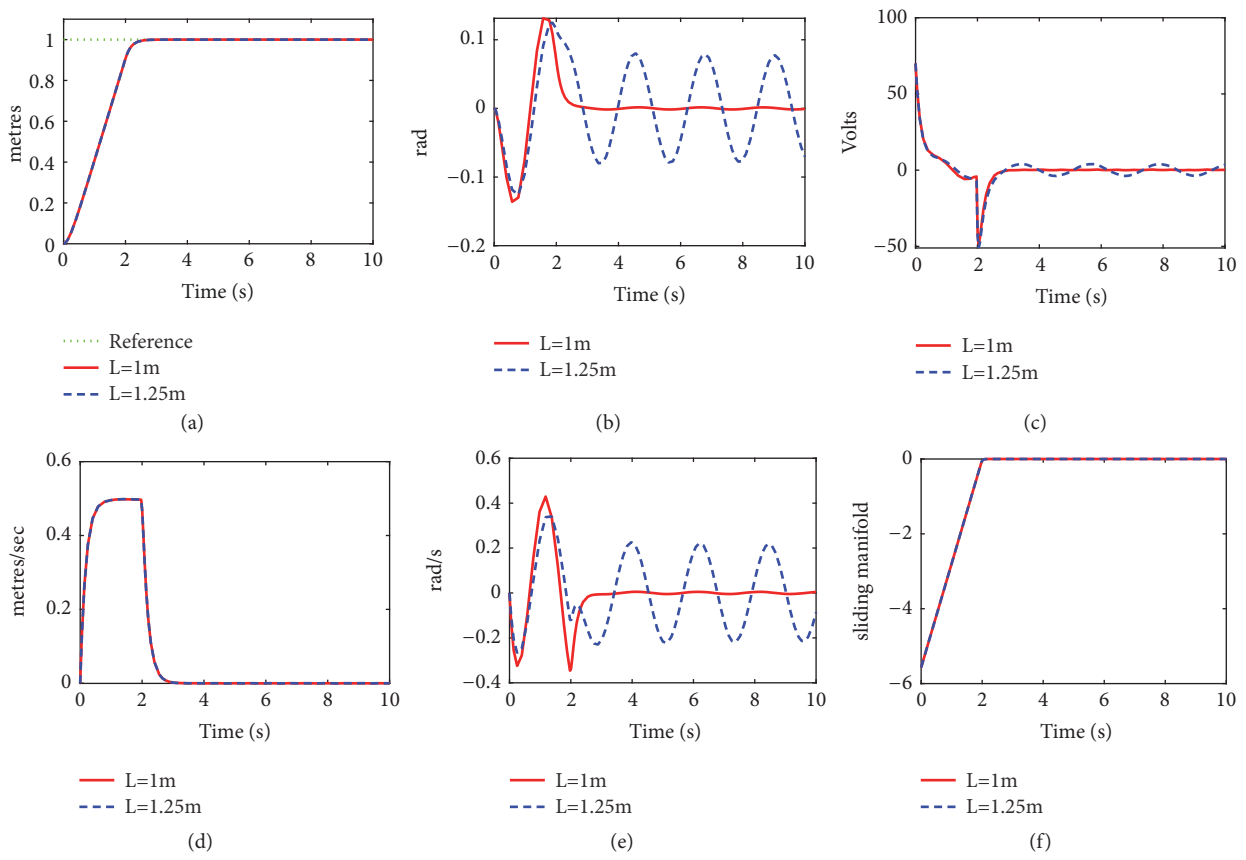

Figure 6: Responses without intelligent tuning algorithms. (a) Cart position. (b) Payload sway. (c) Control effort. (d) Cart velocity. (e) Sway angular velocity. (f) Sliding manifold.

In Figure 6, the performances of the SMC controller without intelligent tuning algorithms for hoisting heights of 1 m and 1.25 m are investigated. A 5 kg load is assumed to be transported to a target position of 1 m. As expected, examining the responses revealed that the payload sways as hoisting height increased from 1 m to 1.25 m. The sway lingers due to the decrease in the crane's ω_n (see (24)). In order to improve the effectiveness of the controller for all operating conditions, fine-tuning of controller is required.

Figure 7 shows the responses obtained when the performance of the controller with intelligent tuning algorithms was investigated. For the purpose of comparison, the same parameters are used as in the previous case (Figure 6). One can see from the responses that the sway has been effectively suppressed despite the changes in hoisting height. Also, the responses of the fuzzy-tuned SMC (FZ-SMC) and the neural-network-tuned SMC (NN-SMC) are overlapping. However, for a quantitative comparison of the performances of the two control strategies, we employ the IAE (see (44)) and the ITAE (see (45)) as criteria. The IAE and ITAE values for Figure 7 correspond to case ID 1 in Table 4 and are for the case when the hoisting height was set to 1.25m. Based on Table 4, the

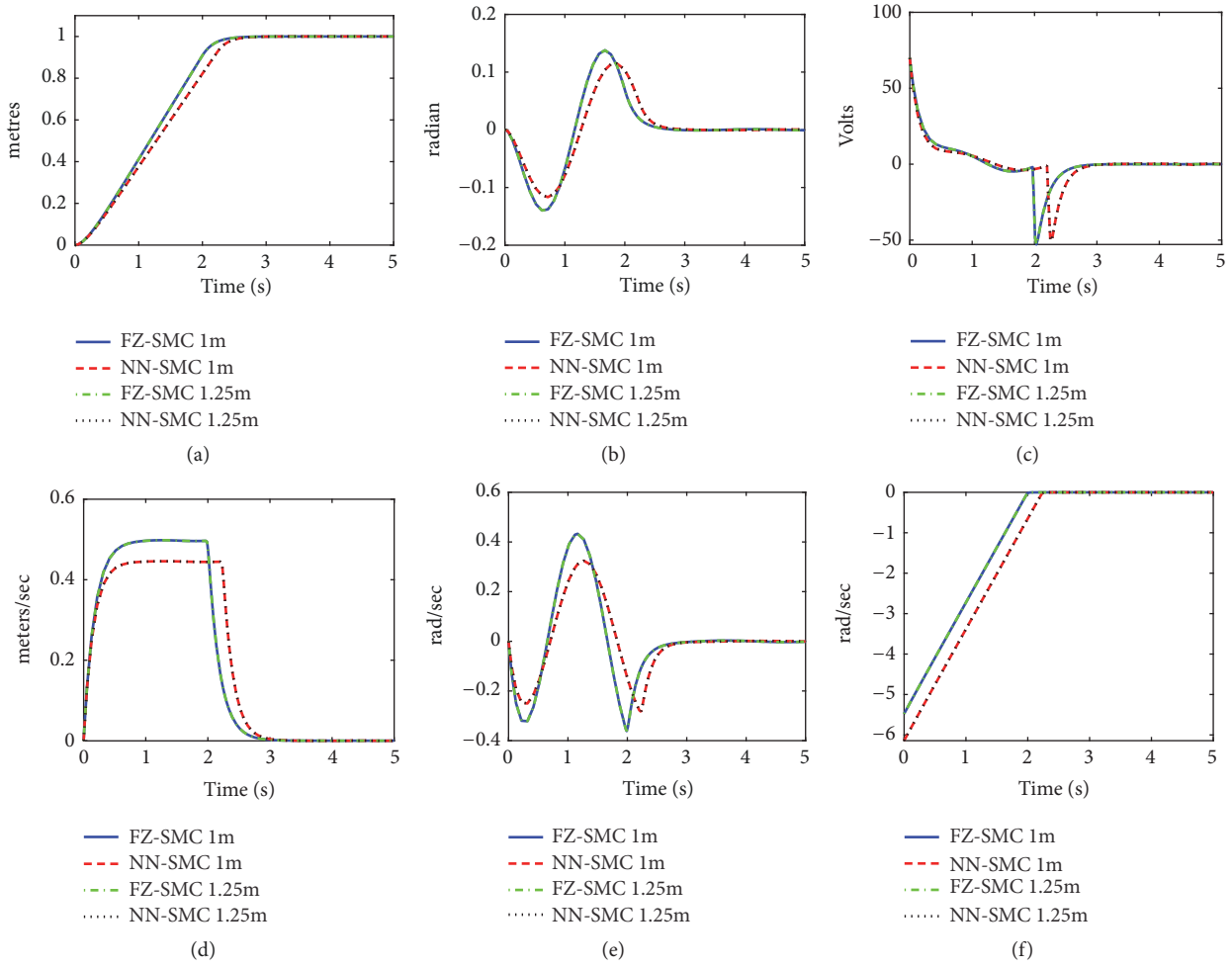

FIGURE 7: Responses with intelligent tuning algorithms. (a) Cart position. (b) Payload sway. (c) Control effort. (d) Cart velocity. (e) Sway angular velocity. (f) Sliding manifold.

performance of the NN-SMC is only slightly better relative to that of the FZ-SMC in terms of sway attenuation.

IAE and ITAE are, respectively, defined by (44) and (45), wherein here $e(\tau)$ refers to the τ^{th} sway regulation error.

$$IAE = \int_0^t |e(\tau)|\, d\tau, \tag{44}$$

$$ITAE = \int_0^t \tau\, |e(\tau)|\, d\tau. \tag{45}$$

Figure 8 shows the case when a payload of 10 kg is transported to a 2 m position from the reference. For the first 10 seconds of operation, it was assumed that the required hoisting height is 1m, and between 10 and 20 seconds the height changed to 1.5 m, while between 20 and 30 seconds the required hoisting height is 0.5 m for obstacle avoidance along the trajectory of the payload. Examining the responses, the performances of the two controllers are effective based on position tracking, minimal acceleration-induced sway, and residual sway suppression capabilities. Furthermore, the control efforts (Figure 8(e)) revealed that the control efforts have attenuated chattering and $\sigma(e,t) = 0$ attained in about 4 seconds (see Figure 8(c)). The IAE and ITAE values for the case studied in Figure 8 correspond to study Case ID 2 in Table 4. Like in the previous control application, the performance of the NN-SMC is only slightly better relative to that of the FZ-SMC in terms of sway attenuation (see Table 4, case ID 2).

Two other control applications were performed (Case ID 3 and 4) to investigate the performances of the proposed control strategies (FZ-SMC and NN-SMC). For brevity, only the IAE and ITAE values for cases are shown in Table 4. Case ID 3 corresponds to the study case when a payload of 20 kg is transported at a fixed hoisting height of 1 m. During the first 10 seconds of operation, the target position is 1 m, and between 10 and 20 seconds of operation the cart is given command to move to the 2 m position, while between 20 and 30 seconds the target position is 3 m. Based on the IAE and ITAE values Case ID 3, the performance of the NN-SMC is slightly better than that of the FZ-SMC like in the previous control applications. On the other hand, Case ID 4 refers to the application when payload of 20 kg is transported. Position tracking for this case is the same as previous control application (Case ID 3). However, for this case, during the

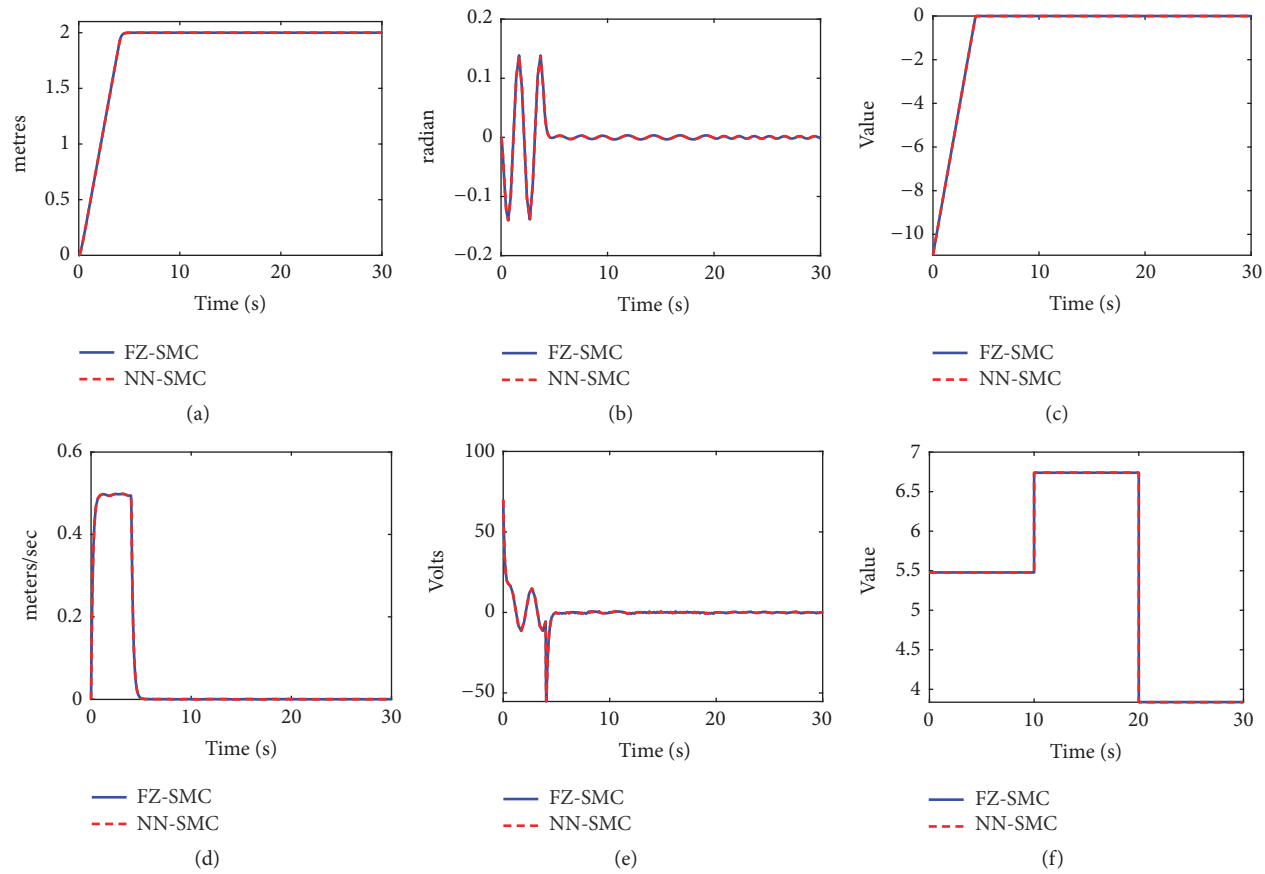

Figure 8: Responses of the FZ-SMC and NN-SMC controllers; (a) cart position, (b) payload sway, (c) sliding manifold, (d) cart velocity, (e) control effort, and (f) manifold slope.

first 10 seconds of operation the cable length is 1 m, and between 10 and 20 seconds the length changed to 1.5 m, while between 20 and 30 seconds the length changed to 0.5 m for obstacle avoidance along the trajectory of the payload. From Table 4, the performance of the NN-SMC is slightly better as compared to that obtained using the FZ-SMC.

Remark 4. In this study, one can argue that both control strategies (FZ-SMC and NN-SMC) are equally effective in dealing with position tracking and sway suppression. However, it is worth noting that the effectiveness of the intelligent algorithms relies heavily on the proper design and training of these algorithms.

So far, we only investigate the effectiveness of the proposed algorithms within the range of the training dataset (0.25 m to 1.5 m). The responses shown in Figure 9 are those obtained for a hoisting height of 1.7 m (i.e., 0.2 m above dataset upper bound). Payload is accepted as 15 kg and target position is 1m. Examining the responses, the NN-SMC remains robust in terms of sway suppression, while the effectiveness of the FZ-SMC deteriorates. This is because the training of the NN based on the back-propagation learning and adaptation algorithm enables it to learn and establish an appropriate functional relationship between training sets. Consequently, the network can effectively predict the optimal values of "slope-updates" for those inputs outside the range of the training dataset. On the other hand, the accuracy of the fuzzy-based tuning algorithm relies heavily on the defined universe of discourse for the input variable as well as the values returned when the MFs are read. In order words, the design of the fuzzy does not account for a hoisting height of 1.7 m. Hence, the fuzzy-based algorithm could not accurately predict the corresponding change in slope for Case ID 5.

Remark 5. For practical cranes, there exists control input saturation problem. Also, the inclusion of integral term in the control law can reduce final positioning errors due to parametric uncertainties or unmodelled dynamics. These two problems might arise in practice and are not considered here. In fact, there is already an effective solution to these problems in [41] that can be applied to practical cranes to solve the problems.

5. Conclusion and Future Work

Payload mass and hoisting height take different values during crane operation. Hence, high-quality control requires robustness against parametric uncertainties. The invariance property of the SMC against matched uncertainty makes it

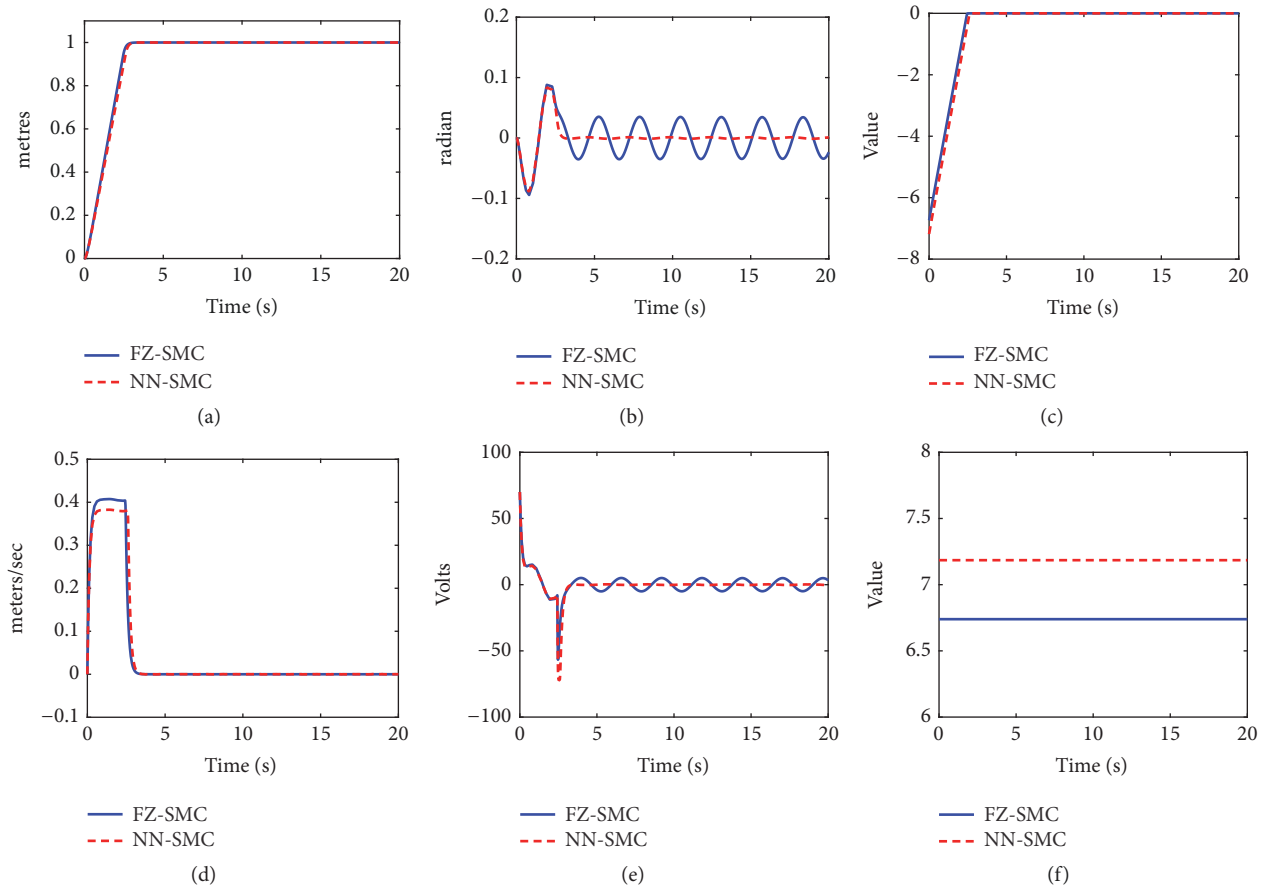

FIGURE 9: Responses for a hoisting height of 1.7m. (a) Cart position. (b) Payload sway. (c) Sliding manifold. (d) Cart velocity. (e) Control effort. (f) Manifold slope.

particularly attractive in control engineering. In this work, the SMC strategy was designed to address the crane control requirements for high-speed of operation, accurate positioning, and minimal sway. To improve the robustness of the proposed SMC strategy, intelligent tuning algorithms based on fuzzy and the NN algorithms were designed to optimize the proposed SMC performance. Controls were repeated by varying payload, position set-point, and hoisting heights in order to demonstrate the quality of the proposed control algorithms to parametric variations. Analyses of performances based on graphical, IAE, and ITAE criteria showed the effectiveness of the proposed methods. However, it was observed based on IAE and ITAE criteria that the NN-SMC strategy was slightly more effective as compared to the FZ-SMC strategy. It was also observed that, for the case of the NN-SMC strategy, there might not be the need for complete redesign of the tuning algorithm in the case where the system requires expansion to cover for higher hoisting heights not considered during control design. Furthermore, attenuated chattering and fast convergence of the sliding variable were observed.

To verify the practical performance of the proposed controllers, experiments can be conducted on an industrial crane. Our next work will be to investigate the effectiveness of the proposed algorithms from practical perspective.

Data Availability

No data were used to support this study.

Conflicts of Interest

The authors declare that there are no conflicts of interest regarding the publication of this paper.

Acknowledgments

The research was supported by the Shaanxi Provincial Key Research and Development Program [Grant No. 2017KW-ZD-04].

References

[1] D. Qian and J. Yi, "Design of combining sliding mode controller for overhead crane systems," *International Journal of Control, Automation and Systems*, vol. 6, no. 1, pp. 131–140, 2013.

[2] H. Jaafar, Z. Mohamed, M. Shamsudin, N. Mohd Subha, L. Ramli, and A. Abdullahi, "Model reference command shaping for vibration control of multimode flexible systems with application to a double-pendulum overhead crane," *Mechanical Systems and Signal Processing*, vol. 115, pp. 677–695, 2019.

[3] A. M. Abdullahi, Z. Mohamed, H. Selamat et al., "Adaptive output-based command shaping for sway control of a 3D overhead crane with payload hoisting and wind disturbance," *Mechanical Systems and Signal Processing*, vol. 98, pp. 157–172, 2018.

[4] V. D. La and K. T. Nguyen, "Combination of input shaping and radial spring-damper to reduce tridirectional vibration of crane payload," *Mechanical Systems and Signal Processing*, vol. 116, pp. 310–321, 2019.

[5] L. Ramli, Z. Mohamed, and H. Jaafar, "A neural network-based input shaping for swing suppression of an overhead crane under payload hoisting and mass variations," *Mechanical Systems and Signal Processing*, vol. 107, pp. 484–501, 2018.

[6] M. Maghsoudi, Z. Mohamed, M. Tokhi, A. Husain, and M. Abidin, "Control of a gantry crane using input-shaping schemes with distributed delay," *Transactions of the Institute of Measurement and Control*, vol. 39, no. 3, pp. 361–370, 2017.

[7] M. J. Maghsoudi, Z. Mohamed, S. Sudin, S. Buyamin, H. Jaafar, and S. Ahmad, "An improved input shaping design for an efficient sway control of a nonlinear 3D overhead crane with friction," *Mechanical Systems and Signal Processing*, vol. 92, pp. 364–378, 2017.

[8] A. Alhassan, K. A. Danapalasingam, M. Shehu, A. M. Abdullahi, and A. Shehu, "Comparing the Performance of Sway Control Using ZV Input Shaper and LQR on Gantry Cranes," in *Proceedings of the 9th Asia International Conference on Mathematical Modelling and Computer Simulation - Asia Modelling Symposium, AMS 2015*, pp. 61–66, Malaysia, September 2015.

[9] M. A. Ahmad, M. S. Ramli, and R. M. Ismail, "Infinite Impulse Response Filter Techniques for Sway Control of a Lab-Scaled Rotary Crane System," in *Proceedings of the 2010 Second International Conference on Computer Modeling and Simulation (ICCMS)*, pp. 192–196, Sanya, China, January 2010.

[10] X. Xie, J. Huang, and Z. Liang, "Vibration reduction for flexible systems by command smoothing," *Mechanical Systems and Signal Processing*, vol. 39, no. 1-2, pp. 461–470, 2013.

[11] R. P. L. Caporali, "Iterative method for controlling with a command profile the sway of a payload for gantry and overhead traveling cranes," *International Journal of Innovative Computing, Information and Control*, vol. 14, no. 3, pp. 1095–1112, 2018.

[12] K. Khandakji1, V. Busher, and L. Melnikova, "Anti-sway system for container cranes with coordinated motion control and reduced dynamic loads," *Jordan Journal of Electrical Engineering*, vol. 3, no. 2, pp. 82–101, 2017.

[13] Z. Wu and X. Xia, "Optimal motion planning for overhead cranes," *IET Control Theory & Applications*, vol. 8, no. 17, pp. 1833–1842, 2014.

[14] L. Ramli, Z. Mohamed, A. M. Abdullahi, H. Jaafar, and I. M. Lazim, "Control strategies for crane systems: A comprehensive review," *Mechanical Systems and Signal Processing*, vol. 85, pp. 1–23, 2017.

[15] H. I. Jaafar, M. F. Sulaima, Z. Mohamed, and J. J. Jamian, "Optimal PID controller parameters for nonlinear gantry crane system via MOPSO technique," in *Proceedings of the 2013 IEEE Conference on Sustainable Utilization and Development in Engineering and Technology (CSUDET)*, pp. 86–91, Selangor, Malaysia, May 2013.

[16] P. A. Ospina-Henao and F. López-Suspes, "Dynamic analysis and control PID path of a model type gantry crane," *Journal of Physics: Conference Series*, vol. 850, p. 012004, 2017.

[17] R. E. Samin and Z. Mohamed, "Comparative assessment of anti-sway control strategy for tower crane system," in *Proceedings of the advances in electrical and electronic engineering: from theory to applications: proceedings of the international conference on electrical and electronic engineering (Ic3e 2017)*, vol. 1883, pp. 1–9, Johor, Malaysia, 2017.

[18] N. Sun, Y. Wu, Y. Fang, and H. Chen, "Nonlinear Antiswing Control for Crane Systems With Double-Pendulum Swing Effects and Uncertain Parameters: Design and Experiments," *IEEE Transactions on Automation Science and Engineering*, vol. 15, no. 3, pp. 1413–1422, 2018.

[19] A. Aksjonov, V. Vodovozov, and E. Petlenkov, "Three-Dimensional Crane Modelling and Control Using Euler-Lagrange State-Space Approach and Anti-Swing Fuzzy Logic," *Electrical, Control and Communication Engineering*, vol. 9, no. 1, pp. 5–13, 2015.

[20] N. M. Bashir, A. A. Bature, and A. M. Abdullahi, "Pole placement control of a 2D gantry crane system with varying pole locations," *Applications of Modeling and Simulation*, vol. 2, no. 1, pp. 8–16, 2018.

[21] Z. Wu, X. Xia, and B. Zhu, "Model predictive control for improving operational efficiency of overhead cranes," *Nonlinear Dynamics*, vol. 79, no. 4, pp. 2639–2657, 2015.

[22] D. T. Liu and W. P. Guo, "Tracking control for an underactuated two-dimensional overhead crane," *Journal of Applied Research and Technology*, vol. 10, no. 4, pp. 597–606, 2012.

[23] Z. Xi and T. Hesketh, "Discrete time integral sliding mode control for overhead crane with uncertainties," *IET Control Theory & Applications*, vol. 4, no. 10, pp. 2071–2081, 2010.

[24] O. Yakut, "Application of intelligent sliding mode control with moving sliding surface for overhead cranes," *Neural Computing and Applications*, vol. 24, no. 6, pp. 1369–1379, 2014.

[25] X. Weimin, Z. Xiang, L. Yuqiang, Z. Mengjie, and L. Yuyang, "Adaptive dynamic sliding mode control for overhead cranes," in *Proceedings of the 2015 34th Chinese Control Conference (CCC)*, pp. 3287–3292, Hangzhou, China, July 2015.

[26] C. Vázquez, L. Fridman, J. Collado, and I. Castillo, "Second-Order Sliding Mode Control of a Perturbed-Crane," *Journal of Dynamic Systems, Measurement, and Control*, vol. 137, no. 8, p. 081010, 2015.

[27] Q. Ngo and K. Hong, "Adaptive sliding mode control of container cranes," *IET Control Theory & Applications*, vol. 6, no. 5, p. 662, 2012.

[28] L. A. Tuan and S. Lee, "Sliding mode controls of double-pendulum crane systems," *Journal of Mechanical Science and Technology*, vol. 27, no. 6, pp. 1863–1873, 2013.

[29] K. Choi and J. S. Lee, "Sliding mode control of overhead crane," *International Journal of Modelling and Simulation*, vol. 31, no. 3, pp. 203–209, 2011.

[30] L. A. Tuan, S.-C. Moon, W. G. Lee, and S.-G. Lee, "Adaptive sliding mode control of overhead cranes with varying cable length," *Journal of Mechanical Science and Technology*, vol. 27, no. 3, pp. 885–893, 2013.

[31] M. Zhang, X. Ma, R. Song et al., "Adaptive proportional-derivative sliding mode control law with improved transient performance for underactuated overhead crane systems," *IEEE/CAA Journal of Automatica Sinica*, vol. 5, no. 3, pp. 683–690, 2018.

[32] L. A. Tuan and S. Lee, "Modeling and advanced sliding mode controls of crawler cranes considering wire rope elasticity and complicated operations," *Mechanical Systems and Signal Processing*, vol. 103, pp. 250–263, 2018.

[33] A. Kareem, *Fuzzy logic based super-twisting sliding mode controllers for dynamic uncertain systems*, St. Peters Institute of Higher Education and Research, St. Peters University, Chennai, India, March 2014.

[34] R. Mar, A. Goyal, V. Nguyen, T. Yang, and W. Singhose, "Combined input shaping and feedback control for double-pendulum systems," *Mechanical Systems and Signal Processing*, vol. 85, pp. 267–277, 2017.

[35] N. M. Tahir, A. G. Ibrahim, and H. Liman, "Hybrid position and vibration control of nonlinear crane system," *Journal of Mechanical Science and Technology*, vol. 9, no. 2, pp. 71–86, 2017.

[36] R. E. Samin, Z. Mohamed, J. Jalani, and R. Ghazali, "A hybrid controller for control of a 3-DOF rotary crane system," in *proceeding of the 2013 First Int. Conf. on Artificial Intell., Modelling Simulation, Kota Kinabalu*, pp. 190–195, Sabah, Malaysia, 2013.

[37] D. Qian and J. Yi, *Hierarchical sliding mode control for under-actuated cranes*, Springer, Berlin, Germany, 2016.

[38] D. E. Rumelhart, G. E. Hinton, and R. J. Williams, "Learning representations by back-propagating errors," *Nature*, vol. 323, no. 6088, pp. 533–536, 1986.

[39] R. Patel and V. Kumar, "Artificial Neuro Fuzzy Logic PID Controller based on BF-PSO Algorithm," *Procedia Computer Science*, vol. 54, pp. 463–471, 2015.

[40] L. X. Hai, T. H. Nguyen, T. G. Khanh, N. T. Thanh, B. T. Duong, and P. X. Minh, "Anti-sway tracking control of overhead crane system based on pid and fuzzy sliding mode control," *Vietnam Journal of Science and Technology*, vol. 55, no. 1, pp. 116–127, 2017.

[41] N. Sun, T. Yang, Y. Fang, Y. Wu, and H. Chen, "Transportation Control of Double-Pendulum Cranes With a Nonlinear Quasi-PID Scheme: Design and Experiments," *IEEE Transactions on Systems, Man, and Cybernetics: Systems*, pp. 1–11, 2018.